Eur. Phys. J. D **15**, 413–422 (2001)

THE EUROPEAN PHYSICAL JOURNAL D

EDP Sciences

Femtosecond pump-probe fluorescence signals from classical trajectories: comparison with wave-packet calculations

V.A. Ermoshin[1] and V. Engel[2,a]

[1] Fock Institute of Physics, The University of St. Petersburg, 198504 St. Petersburg, Russia
[2] Institut für Physikalische Chemie, Universität Würzburg, Am Hubland, 97074 Würzburg, Germany

Received 28 March 2001

Abstract. A classical approach to simulate femtosecond pump-probe experiments is presented and compared to the quantum mechanical treatment. We restrict the study to gas-phase systems using the I_2 molecule as a numerical example. Thus, no relaxation processes are included. This allows for a direct comparison between purely quantum mechanical results and those obtained from classical trajectory calculations. The classical theory is derived from the phase-space representation of quantum mechanics. Various approximate quantum mechanical treatments are compared to their classical counterparts. Thereby it is demonstrated that the representation of the radial density as prepared in the pump-process is most crucial to obtain reliable signals within the classical approach.

PACS. 31.70.Hq Time-dependent phenomena: excitation and relaxation processes, and reaction rates – 33.80.Wz Other multiphoton processes

1 Introduction

Time-resolved spectroscopy of molecules is a powerful technique for the investigation of photo-induced dynamical processes [1–6]. The use of ultrashort laser pulses allows for the preparation of an ensemble of molecules in a coherent superposition of ro-vibrational or translation states, *i.e.* a nuclear wave packet [7]. Since such a wave packet represents a non-stationary state of the system under investigation, observables are inherently time-dependent. Interrogating the sample with a time-delayed second pulse then allows to monitor the quantum dynamics of the system.

From a theoretical point of view, quantum mechanical calculations of time-resolved signals for isolated small molecules are straightforward. Unfortunately this is not the case for larger molecules or molecules interacting with a multi-particle environment. Here, clearly, one is forced to employ approximate methods. Concerning the numerical effort, a classical approach is highly advantageous; furthermore such a description is truly *ab initio* in the sense that all interactions can be incorporated without any limitation.

In recent time much attention has been paid to the calculation of pump-probe fluorescence signals from classical trajectories [8–14]. Other classical approaches were used for the simulation of coherent non-linear spectroscopy (see, *e.g.* Refs. [15–17]) which will, however, not be addressed in what follows. This strategy seems to be successful for the simulation of femtosecond spectroscopy if not too long time periods are regarded. For heavier atoms, quantum-mechanical effects are substantial only at longer times [18]; on the other hand, in the case of a system-bath coupling, the interaction with the environment leads to the loss of coherence of the molecular wave packet thus reducing the importance of quantum-mechanical effects.

Whereas many observables can, to a very good approximation, be calculated classically [19] the principal problem associated with classical trajectory calculations of time-resolved signals is how to incorporate the laser-induced transitions between molecular electronic states into the classical scheme. Regarding a transition from the electronic state $|g\rangle$ to an excited state $|e\rangle$, the simplest scheme is to start all trajectories from the point $\bar{r}$ defined by the resonance condition $U_e(\bar{r}) - U_g(\bar{r}) = \hbar\omega_{\rm pump}$ [20], where U_e, U_g are the respective potential curves. This approximation neglects the spatial extent of the initial wave-packet as well as the finite temporal width of the femtosecond pump-pulse. Nevertheless, a qualitative description of the pump-probe spectroscopy is provided within this simple approach.

An incorporation of the pulse temporal width can be performed using first order time-dependent perturbation theory neglecting all kinetic energy operators which appear in the expression for the excited state wave function [21]. The latter then is a product of the initial state and a r-dependent window function $F(r)$. The corresponding classical distribution is obtained by sampling from the quantum density. This approximation can be applied for

[a] e-mail: voen@phys-chemie.uni-wuerzburg.de

relatively short laser pulses, but for commonly employed pulses, having widths in the order of 100 fs it is likely to fail. A classical method which takes the molecular motion during the pulse excitation into account has been proposed by Martens and co-workers [8]. Using a time-integral representation for the density matrix the authors constructed classical densities which depend on both the spectral (through the function $F(r)$) and temporal variables. Shen and Cina [9] introduced a classical scheme including the case of overlapping pump- and probe-pulses.

The important work of Li *et al.* [8] uses the density-matrix formalism which provides a direct correspondence between quantum-mechanical and classical densities. This is necessary if one is interested in processes where a system-bath interaction is of importance. The primary goal of the present paper is to arrive at a classical approach to calculate pump-probe fluorescence signals using wave functions as a starting point. Since a quantum mechanical phase space distribution is obtained *via* the Wigner transformation [22–24] we use this approach to set up the classical description. In order to judge on the results of the classical calculations they are compared to those obtained from quantum calculations.

The paper is organized as follows. In Section 2 we consider the exact and approximate quantum-mechanical treatment of pump-probe experiments. A classical approach is presented in Section 3. We test the theory and discuss the results in Section 4 and concluding remarks are contained in Section 5.

2 Quantum-mechanical treatment

2.1 General considerations

Let us regard a diatomic molecule with reduced mass m, an electronic ground state $|g\rangle$ and two excited states $|e\rangle, |f\rangle$. For simplicity we treat only a single nuclear degree-of-freedom with vibrational coordinate r. Our description of the pump- and probe-transition is based on first-order time-dependent perturbation theory which applies in the limit of weak laser intensities. Starting, at time $t = 0$, from the initial wave function $\Psi_g(r)$ in the electronic ground state, the nuclear wave function in state $|e\rangle$ which is prepared in the pump-process is given as

$$\Psi_e(r,t_2) = -\frac{\mathrm{i}}{\hbar}\int_0^{t_2} \mathrm{d}t\ \mathrm{e}^{-\mathrm{i}H_e(t_2-t)/\hbar} W_1(r,t) \times \mathrm{e}^{-\mathrm{i}H_g t/\hbar}\Psi_g(r), \quad (1)$$

where $H_{g,e}$ denote the Hamiltonians for the nuclear motion in the two electronic states. The molecule-field interaction, within the dipole approximation, takes the form

$$W_1(r,t) = -\frac{\mu_{ge}}{2} f(t)\mathrm{e}^{-\mathrm{i}\omega_1 t}, \quad (2)$$

where μ_{ge} denotes the projection of the transition dipole-moment (for the $|e\rangle \leftarrow |g\rangle$ transition) on the polarization vector of the electric field and we kept only the resonant term leading to photon absorption. In what follows, we set $\mathrm{i}\mu_{ge}/2\hbar = 1$, thereby assuming a constant dipole moment (Condon approximation) and neglecting irrelevant phase factors. Since below we calculate only populations and no absolute numbers, this convention is reasonable.

The pump laser-pulse is characterized by its frequency ω_1 and a temporal shape function which we assume to be a Gaussian: $f(t) = \exp\left(-(t-t_\mathrm{c})^2/2\tau^2\right)$. The integration interval $[0, t_2]$ is chosen such that $t_\mathrm{c} = t_2/2$ and $f(t)$ is sufficiently small at the boundaries. This implies that only times t_2 are considered for which the pump-excitation has finished.

Insertion of equation (2) into equation (1) and back-propagation from time t_2 to the time origin yields

$$\Psi_e(r,0) = \int_0^\infty \mathrm{d}t\ f(t)\mathrm{e}^{\mathrm{i}(H_e-\hbar\omega_1)t/\hbar}\mathrm{e}^{-\mathrm{i}H_g t/\hbar}\Psi_g(r), \quad (3)$$

where the integration is over the entire real axis. The wave function for times t_2, after the pump-process is finished, then is simply given as $\Psi_e(r,t_2) = \mathrm{e}^{-\mathrm{i}H_e t_2/\hbar}\Psi_e(r,0)$.

Let us next turn to the probe excitation to state $|f\rangle$, which is induced by a second laser pulse, delayed by time t_d with respect to the pump-pulse. Giving the interaction energy as

$$W_2(r,t) = -\frac{\mu_{fe}}{2} f(t-t_\mathrm{d})\mathrm{e}^{-\mathrm{i}\omega_2(t-t_\mathrm{d})}, \quad (4)$$

and applying the same approximations as above, the nuclear wave function in the electronic state $|f\rangle$ can be written as

$$\Psi_f(r,t_\mathrm{d}) = \int_0^\infty \mathrm{d}t\ f(t)\mathrm{e}^{\mathrm{i}(H_f-\hbar\omega_2)t/\hbar}\mathrm{e}^{-\mathrm{i}H_e t/\hbar}\Psi_e(r,t_\mathrm{d}). \quad (5)$$

The fluorescence signal $S(t_\mathrm{d})$ from state $|f\rangle$ is assumed to be proportional to the population in this state after the probe pulse passed the sample:

$$S(t_\mathrm{d}) = \langle\Psi_f(r,t_\mathrm{d})|\Psi_f(r,t_\mathrm{d})\rangle\cdot \quad (6)$$

We will refer to the approach presented in this subsection as to the "exact" calculation.

2.2 Approximate calculation of pump-probe signals

The numerical calculation of the pump-probe signal is, in principle, straightforward. Nevertheless, if the signal is required for a long time and especially if several degrees-of-freedom have to be treated, the calculation becomes cumbersome. This, in particular, applies to the treatment of the probe transition. Several approximations can now be introduced as will be described in what follows. We note that the approximations given below are not new and have been used in one or the other form by many authors. Here we give the corresponding equations to make contact to the classical formalism. Various levels of accuracy are included and the resulting approximations are named accordingly for convenience.

Inserting equation (5) into equation (6), the pump-probe signal can be written as

$$S(t_{\rm d}) = \int_0^\infty {\rm d}t\ f(t) \int_0^\infty {\rm d}t' f(t') {\rm e}^{{\rm i}\omega_2(t-t')} \times \left\langle \Psi_e(r,t_{\rm d}) | U^\dagger(t) U(t') | \Psi_e(r,t_{\rm d}) \right\rangle, \quad (7)$$

where the propagator $U(t)$ is defined as

$$U(t) = {\rm e}^{{\rm i}H_f t/\hbar} {\rm e}^{-{\rm i}H_e t/\hbar}. \quad (8)$$

The double integral in equation (7) can be evaluated using the approximation [25]

$${\rm e}^{{\rm i}H_f t/\hbar} {\rm e}^{-{\rm i}H_e t/\hbar} \approx {\rm e}^{{\rm i}(H_f - H_e)t/\hbar} {\rm e}^{1/2[H_f,H_e](t/\hbar)^2}, \quad (9)$$

where higher order terms in $t/\hbar$ were omitted. Neglecting the commutator $[H_f, H_e]$ in the latter equation yields an expression for the $|f\rangle$-state wave function as [21]:

$$\Psi_f^{\rm SF}(r,t_{\rm d}) = \int_0^\infty {\rm d}t\ f(t) {\rm e}^{{\rm i}(\Delta_{fe}(r) - \hbar\omega_2)t/\hbar} \Psi_e(r,t_{\rm d}). \quad (10)$$

Here the difference $\Delta_{fe}(r) = U_f(r) - U_e(r)$ between the potentials in the electronic state $|f\rangle$ and $|e\rangle$ was introduced.

Analytical evaluation of the Gaussian integral (10) gives

$$\Psi_f^{\rm SF}(r,t_{\rm d}) = F_2(r) \Psi_e(r,t_{\rm d}), \quad (11)$$

with the spatial window defined as

$$F_2(r) = \sqrt{2\pi}\tau \exp\left(-\frac{\tau^2(\Delta_{fe}(r) - \hbar\omega_2)^2}{2\hbar^2} \right). \quad (12)$$

In deriving equation (12) we have ignored a phase factor which arises since the probe-pulse Gaussian envelope is not centered around $t = 0$. This is, however, not relevant for the pump-probe signal, see equation (6). Thus, within the above approximation, the $|f\rangle$-state wave-function is obtained by the product of $\Psi_e(r,t_{\rm d})$ with the r-dependent window, thus we use the abbreviation SF which stands for spatial filtering. The signal then takes the simple form

$$S^{\rm SF}(t_{\rm d}) = \left\langle \Psi_e(r,t_{\rm d}) | F_2^\dagger(r) F_2(r) | \Psi_e(r,t_{\rm d}) \right\rangle. \quad (13)$$

The latter expression for the pump-probe signals appeals to the central idea of pump-probe spectroscopy: the signal measures a probability density, located in a restricted area of configuration space. Since the density is time-dependent, temporal changes of the signal directly map the quantum dynamics. We note that the above described approximation, namely the neglect of the kinetic energy operators has also been used in deriving *e.g.* the reflection principle of cw-absorption spectroscopy; for an extended discussion see the book of Schinke and references therein [26].

The SF approximation does not account for the wave-packet motion during the laser excitation-process. This motion can be incorporated by approximation of the commutator $[H_f, H_e] = [T, \Delta_{fe}(r)]$, where $T = p^2/2m$ is the kinetic energy operator [27–29]. Evaluation of the commutator yields

$$[T, \Delta_{fe}(r)] = -\frac{{\rm i}\hbar}{2m} \left(2\Delta'_{fe}(r) p + \Delta''_{fe}(r) \right), \quad (14)$$

where $\Delta'_{fe}(r)$ is the derivative of $\Delta_{fe}(r)$ with respect to r, and $\Delta''_{fe}(r)$ denotes the second derivative. The approximation now consists in the substitution of the momentum operator p by its mean value $\overline{p} = \langle \Psi_e | p | \Psi_e \rangle$, resulting in

$$[T, \Delta_{fe}(r)] \approx -\frac{{\rm i}\hbar\overline{p}\Delta'_{fe}(r)}{m}, \quad (15)$$

where we, for simplicity, assumed a linear difference potential. The equation for the final state wave function in this "mean momentum" (MM) approximation reads

$$\Psi_f^{\rm MM}(r,t_{\rm d}) = \int_0^\infty {\rm d}t\ f(t) {\rm e}^{{\rm i}(\Delta_{fe}(r) - \hbar\omega_2)t/\hbar} \times {\rm e}^{-{\rm i}\beta(r,\overline{p})t^2/\hbar^2} \Psi_e(r,t_{\rm d}), \quad (16)$$

where $\beta(r,\overline{p}) = \hbar\overline{p}\Delta'_{fe}(r)/2m$. Again, we encounter a Gaussian integral leading to the expression (ignoring a phase factor, as above)

$$\Psi_f^{\rm MM}(r,t_{\rm d}) = G_2(r,\overline{p}) \Psi_e(r,t_{\rm d}), \quad (17)$$

where we used the definition

$$G_2(r,\overline{p}) = \sqrt{\frac{2\pi\tau^2}{1 + 2{\rm i}\tau^2\beta(r,\overline{p})/\hbar^2}} \times \exp\left(-\frac{\tau^2(\Delta_{fe}(r) - \hbar\omega_2)^2}{2\hbar^2(1 + 2{\rm i}\tau^2\beta(r,\overline{p})/\hbar^2)} \right). \quad (18)$$

As in the SF case (see Eq. (11)), within the MM approximation the wave function $\Psi_f(r,t_{\rm d})$ is obtained by multiplication of $\Psi_e(r,t_{\rm d})$ with an r-dependent factor which, however, additionally depends on the mean momentum of the vibrational wave packet in the $|e\rangle$ state. The corresponding signal then is of the form

$$S^{\rm MM}(t_{\rm d}) = \left\langle \Psi_e(r,t_{\rm d}) | G_2^\dagger(r,\overline{p}) G_2(r,\overline{p}) | \Psi_e(r,t_{\rm d}) \right\rangle. \quad (19)$$

The MM approximation will, in general, yield more accurate results than the SF approximation since the commutator $[H_e, H_f]$ is taken into account. However, this is not done exactly and problems are to be expected at *e.g.* the turning points of the vibrational motion where $\overline{p} \sim 0$. Here the SF and MM approximations yield identical results.

A solution which, in calculating the pump-probe signals, incorporates the commutator $[H_f, H_e]$ in a more accurate way was proposed in reference [11]. In what follows we will refer to this approach as the spatiotemporal filtering approximation (STF), for reasons that will become apparent soon. Using new variables $t_1 = t - t'$ and $t_2 = (t + t')/2$, the propagator (8) can be written as

$$U(t) = {\rm e}^{{\rm i}H_f t_2/\hbar} {\rm e}^{{\rm i}H_f t_1/(2\hbar)} {\rm e}^{-{\rm i}H_e t_1/(2\hbar)} {\rm e}^{-{\rm i}H_e t_2/\hbar}; \quad (20)$$
$$U(t') = {\rm e}^{{\rm i}H_f t_2/\hbar} {\rm e}^{-{\rm i}H_f t_1/(2\hbar)} {\rm e}^{{\rm i}H_e t_1/(2\hbar)} {\rm e}^{-{\rm i}H_e t_2/\hbar},$$

so that

$$U^\dagger(t)U(t') = \mathrm{e}^{\mathrm{i}H_e t_2/\hbar}\Big[\mathrm{e}^{\mathrm{i}H_e t_1/(2\hbar)}\mathrm{e}^{-\mathrm{i}H_f t_1/\hbar}\mathrm{e}^{\mathrm{i}H_e t_1/(2\hbar)}\Big] \times \mathrm{e}^{-\mathrm{i}H_e t_2/\hbar}. \quad (21)$$

The operator product appearing in the square brackets of equation (21) can be approximated to third order in $t_1/\hbar$ yielding

$$U^\dagger(t)U(t') \approx \mathrm{e}^{\mathrm{i}H_e t_2/\hbar}\mathrm{e}^{-\mathrm{i}(H_f-H_e)t_1/\hbar}\mathrm{e}^{-\mathrm{i}H_e t_2/\hbar}. \quad (22)$$

Using the property of the product of two Gaussians: $f(t)f(t') = f(t_1/\sqrt{2})f(\sqrt{2}t_2)$ in equation (7) one obtains

$$S^{\mathrm{STF}}(t_\mathrm{d}) = \int_0^\infty \mathrm{d}t_2\ f(\sqrt{2}t_2)\int_{-\infty}^\infty \mathrm{d}t_1\ f\left(\frac{t_1}{\sqrt{2}}\right) \times \left\langle \Psi_e(r,t_2)|\mathrm{e}^{-\mathrm{i}(\Delta_{fe}(r)-\omega_2)t_1/\hbar}|\Psi_e(r,t_2)\right\rangle. \quad (23)$$

Finally, integration over t_1 yields

$$S^{\mathrm{STF}}(t_\mathrm{d}) = \int_0^\infty \mathrm{d}t_2\, f(\sqrt{2}t_2)\langle\Psi_e(r,t_2)|\tilde{F}_2(r)|\Psi_e(r,t_2)\rangle, \quad (24)$$

where

$$\tilde{F}_2(r) = 2\tau\sqrt{\pi}\mathrm{e}^{-\frac{\tau^2(\Delta_{fe}(r)-\hbar\omega_2)^2}{\hbar^2}}. \quad (25)$$

Note that since the time–integrals in the last two expressions start at $t_1 = t_2 = 0$ and in the above equations $|\Psi_e(r, t_1 = t_2 = 0)\rangle \equiv |\Psi_e(r, t_\mathrm{d})\rangle$.

Evaluating the signal using equation (24) does not need an explicit treatment of the probe excitation. It is similar to the expression of equation (13) but now, the exact time-evolution of the $|e\rangle$-state wave packet enters and the signal is obtained as a weighted time average. A formula similar to equation (24) was also obtained in reference [8].

In summary, applying any of the three described approximations (SF, MM, STF) in the quantum-mechanical calculation of pump-probe signals does not require a propagation of a wave packet in the final state $|f\rangle$ hence leading to a considerable saving of computer time. Moreover, in the next section we show that these approximations serve as a starting point for a classical evaluation of pump-probe signals.

3 Classical treatment

3.1 General considerations

To obtain a classical scheme to calculate pump-probe signals, we start with the phase-space formulation of quantum mechanics. Given the wave function $\Psi(r)$ a phase-space distribution can be calculated as the Wigner transform [22–24]

$$D(r,p) = \frac{1}{\pi\hbar}\int \mathrm{d}y\, \Psi(r-y)^*\Psi(r+y)\mathrm{e}^{-2\mathrm{i}py/\hbar}. \quad (26)$$

The expectation value of any operator A then is obtained as

$$\langle A\rangle_{qm} = \int \mathrm{d}r \int \mathrm{d}p\ A_W(r,p)D(r,p), \quad (27)$$

where we used the definition

$$A_W(r,p) = 2\int \mathrm{d}y\ \langle r+y|A|r-y\rangle \mathrm{e}^{-2\mathrm{i}py/\hbar}. \quad (28)$$

In particular, if A depends on r only, $A_W(r) = A(r)$ [30]. Another important case is the density operator. In our treatment of pure states it has the form [31] $\Gamma = (1/2\pi\hbar)|\Psi\rangle\langle\Psi|$. Calculation of its Wigner transform *via* equation (28) obviously leads to equation (26).

The Wigner transform of an operator product $(A(r,p)\,B(r,p))_W$ is of the form

$$(A(r,p)\,B(r,p))_W = \mathrm{e}^{\mathrm{i}\hbar/2(\partial_p^B\partial_r^A - \partial_r^B\partial_p^A)} \times A_W(r,p)B_W(r,p), \quad (29)$$

and assumes a simple form only if one sets $\hbar = 0$ in the exponential operator [30]. Adopting this approximation (as we will do in what follows) the product of three operators transforms as

$$(ABC)_W = (A)_W(B)_W(C)_W, \quad (30)$$

in accordance with classical mechanics. In the special case that A and C are functions of the position operator $\hat{r}$ only and $B = \Gamma = (1/2\pi\hbar)|\Psi\rangle\langle\Psi|$ one obtains

$$(A(\hat{r})\Gamma C(\hat{r}))_W = A(r)D_\Psi(r,p)C(r). \quad (31)$$

A dynamical equation for the phase space density (26) is derived as [22–24,32]

$$\frac{\mathrm{d}}{\mathrm{d}t}D(r,p) = \left(\frac{p}{m}\frac{\partial}{\partial q} + \frac{\partial V}{\partial q}\frac{\partial}{\partial p}\right)D(r,p) + \sum_{j=3,5,\ldots}\frac{1}{j!}\left(\frac{\mathrm{i}\hbar}{2}\right)^{(j-1)}\frac{\partial^j V}{\partial q^j}\frac{\partial^j D(r,p)}{\partial p^j}. \quad (32)$$

By inspection of the equation of motion (32) it should be immediately clear that a general solution, even numerically, is difficult to obtain, see *e.g.* [33–35]. However, two useful facts appear: (i) in the limit ($\hbar \to 0$) the dynamical equation assumes the form of the classical Liouville equation; and (ii) for a quadratic potential, the quantum equation exactly corresponds to the classical one. As a consequence of the latter situation, given an initial density, the quantum mechanical and classical densities move identically [32].

We now look for a convenient representation of the time-dependent phase space-density. First we use the fact that the solution of the classical Liouville equation starting with an initial delta-function $\delta(r-r_0, p-p_0)$ remains a delta-function $\delta(r-r(t), p-p(t))$, where $r(t)$ and $p(t)$

are found from Hamilton's equations of motion [32]. Furthermore we use Monte-Carlo sampling to obtain

$$D(r,p,t) = \frac{1}{N}\sum_{i=1}^{N} \delta(r - r_i(t), p - p_i(t)) D(r_0^i, p_0^i). \quad (33)$$

Here N is the number of sampling points (r_0^i, p_0^i) in phase space that are used as initial conditions for the classical equations of motion.

The initial function $D(r_0, p_0)$ can be the Wigner transform of the initial quantum mechanical wave function or can be a classical thermal distribution function; in equation (33) it naturally appears as a function which defines weights for the sampling points. The time-dependence now is contained only in the δ-functions. Thus, the time-evolution of any classical density can be monitored by solving the classical equations of motion instead of solving the Liouville equation. Note, however, that this is an approximation for the evolution of the quantum-mechanical systems since the equation of motion (32) in general is much more complicated, for a careful discussion see *e.g.* [32].

3.2 The pump-transition

The phase-space distribution prepared in the pump process is obtained from the Wigner transform of the wave function $\Psi_e(r)$ in the excited state $|e\rangle$ (Eq. (3)). The latter can be evaluated exactly as well as approximately. Since for longer excitation pulses the Wigner function, in general, has an oscillating structure (see below) it is not a good sampling function. To calculate the initial $|e\rangle$-state density we will, in what follows, employ the approximation equation (30). Applying the SF approximation to the pump transition (see Eq. (11)) and using equation (31) yields

$$D_e^{\mathrm{SF}}(r,p) = \Big[F_1(\hat{r}) \Gamma_g F_1^\dagger(\hat{r})\Big]_W = F_1^2(r) D_g(r,p), \quad (34)$$

where

$$F_1(r) = \sqrt{2\pi}\tau \mathrm{e}^{-\frac{\tau^2(\Delta_{eg}(r) - \hbar\omega_1)^2}{2\hbar^2}}. \quad (35)$$

Here $\Delta_{eg}(r)$ denotes the difference between the potentials in state $|e\rangle$ and $|g\rangle$. Equation (34) defines a distribution function to sample initial conditions for a set of N trajectories, all starting at the same time $t = 0$. The subsequent time-evolution is obtained by solving the classical equations of motion.

As it was already noted above, the SF-approximation does not account for the nuclear motion during the optical transition. The MM approximation (Sect. 2.2) will not be of advantage here since the mean momentum in the initial vibrational state is zero. Instead we incorporate the motion in the excited state by a time sampling (ts), as was done in the STF approximation which was discussed in connection with the quantum mechanical evaluation of pump-probe signals (Sect. 2.2). In order to do so, let us start with the general expression for the $|e\rangle$-state density operator after the pump-pulse action

$$\Gamma_e(t=0) = \int_0^\infty \mathrm{d}t f(t) \int_0^\infty \mathrm{d}t' f(t') \mathrm{e}^{-\mathrm{i}\omega_1(t-t')} \times U(t) \Gamma_g U^\dagger(t'). \quad (36)$$

The propagators, using the variables $t_1 = t - t'$ and $t_2 = (t + t')/2$, read

$$U(t) = \mathrm{e}^{\mathrm{i}H_e t_2/\hbar}\Big[\mathrm{e}^{\mathrm{i}H_e t_1/(2\hbar)}\mathrm{e}^{-\mathrm{i}H_g t_1/(2\hbar)}\Big]\mathrm{e}^{-\mathrm{i}H_g t_2/\hbar} \approx \mathrm{e}^{\mathrm{i}H_e t_2/\hbar}\mathrm{e}^{\mathrm{i}\Delta_{eg}(r) t_1/(2\hbar)}\mathrm{e}^{-\mathrm{i}H_g t_2/\hbar}, \quad (37)$$

$$U(t') = \mathrm{e}^{\mathrm{i}H_e t_2/\hbar}\Big[\mathrm{e}^{-\mathrm{i}H_e t_1/(2\hbar)}\mathrm{e}^{\mathrm{i}H_g t_1/(2\hbar)}\Big]\mathrm{e}^{-\mathrm{i}H_g t_2/\hbar} \approx \mathrm{e}^{\mathrm{i}H_e t_2/\hbar}\mathrm{e}^{-\mathrm{i}\Delta_{eg}(r) t_1/(2\hbar)}\mathrm{e}^{-\mathrm{i}H_g t_2/\hbar}, \quad (38)$$

where we approximated the terms in the square brackets by neglecting commutators of the form $[T, \Delta_{eg}]$. Since Ψ_g is an eigenstate of H_g, the action of the propagator $\mathrm{e}^{-\mathrm{i}H_g t_2/\hbar}$ leaves the density operator $\Gamma_g = (1/2\pi\hbar)|\Psi_g\rangle\langle\Psi_g|$ invariant. Thus, equation (36) reads

$$\Gamma_e(t=0) = \int_0^\infty \mathrm{d}t_2\, f(\sqrt{2}t_2) \int_{-\infty}^\infty \mathrm{d}t_1\, f\left(\frac{t_1}{\sqrt{2}}\right) \mathrm{e}^{\mathrm{i}H_e t_2/\hbar} \times A\, \mathrm{e}^{-\mathrm{i}H_e t_2/\hbar}, \quad (39)$$

where we introduced the operator

$$A = \mathrm{e}^{\mathrm{i}(\Delta_{eg}(r) - \hbar\omega_1)t_1/(2\hbar)} \Gamma_g\, \mathrm{e}^{\mathrm{i}(\Delta_{eg}(r) - \hbar\omega_1)t_1/(2\hbar)}. \quad (40)$$

The operator $A^{(H)} = \mathrm{e}^{\mathrm{i}H_e t_2/\hbar} A\, \mathrm{e}^{-\mathrm{i}H_e t_2/\hbar}$, appearing in equation (39) is a time-dependent operator in the Heisenberg representation, thus it fulfills the Heisenberg equation of motion [25]

$$\frac{\mathrm{d}A^{(H)}}{\mathrm{d}t} = \frac{1}{\mathrm{i}\hbar}\big[A^{(H)}, H_e\big]. \quad (41)$$

The phase-space analogue of this equation is equation (32), and the classical limit amounts to integration of the classical Liouville equation for the corresponding distribution function [31]. The latter can be obtained using equation (31) as

$$A_{\mathrm{cl}} = \mathrm{e}^{\mathrm{i}(\Delta_{eg}(r) - \hbar\omega_1)t_1/(2\hbar)} D_g(r,p) \mathrm{e}^{\mathrm{i}(\Delta_{eg}(r) - \hbar\omega_1)t_1/(2\hbar)}. \quad (42)$$

Performing the integration over t_1 we obtain for the distribution function corresponding to the operator Γ_e

$$D_e(r,p,t=0) = \int_0^\infty \mathrm{d}t_2\, f\left(\sqrt{2}t_2\right)\Big[\tilde{F}_1(r) D_g(r,p)\Big]_{t_2}, \quad (43)$$

where

$$\tilde{F}_1(r) = 2\tau\sqrt{\pi}\exp\left(-\frac{\tau^2(\Delta_{eg}(r) - \hbar\omega_1)^2}{\hbar^2}\right). \quad (44)$$

The subscript t_2 appearing in equation (43) refers to a propagation in the $|e\rangle$ state and indicates that

$[\tilde{F}_1(r)D_g(r,p)]_{t_2}$ consists of trajectories which started at time t_2 during the pump-pulse excitation but have been propagated back in time to the origin $t = 0$. The integral over t_2 in equation (43) can be evaluated by Monte-Carlo sampling, where the distribution function $f(\sqrt{2}t)\,[\tilde{F}_1(r)\,D_g(r,p)]_t$ now depends on time. Note that the time sampling has to be performed for the finite length of the pump-pulse interaction only.

3.3 The probe-transition

The initial classical density may now be propagated by solving the classical equations of motion (see Eq. (33)). In order to calculate the pump-probe signal let us regard the density at a time t after the pump-pulse interaction. By inspection of the quantum mechanical expressions for the signal, obtained in the various approximations (Eqs. (13, 19, 24)), we note that the signal in each case is related to the expectation value of an r-dependent operator. Using the expression for an expectation value within the phase-space formulation (Eq. (27)) we obtain classical expressions for the signals. Below we give only the most accurate STF formula for the signal which is also used in our numerical examples. The corresponding expressions in the SF- and MM-approximation are readily obtained.

$$S_{\rm cl}^{\rm STF}(t_{\rm d}) = \int_0^\infty {\rm d}t\, f(\sqrt{2}t) \int {\rm d}r \int {\rm d}p\, \tilde{F}_2(r) D_e(r,p,t). \quad (45)$$

Analogous to the quantum mechanical expression equation (24) we have $D_e(r,p,t=0) \equiv D_e(r,p,t=t_{\rm d})$.

Since the classical density in equation (45) is represented as a weighted sum of delta-functions (see Eq. (33)), the integration transforms to the summation of $\tilde{F}_2(r_i(t))$ weighted by the distribution function D_e. Here the coordinates $r_i(t)$ are solutions of Newton's equation with initial conditions sampled from D_e. In equation (45), an additional convolution with pulse shape function should be carried out at the end of the Monte-Carlo integration.

4 Numerical examples

4.1 Description of the model

We use the isolated I_2 molecule at a temperature of 0 K as a model system. Pump-probe fluorescence experiments have been carried out by Zewail and coworkers [36–38]. In these experiments, a first ultrashort laser pulse prepares a wave packet in the electronic state $|e\rangle$ (the B-state), see Figure 1. The time-delayed probe pulse excites the molecule into an ion-pair state $|f\rangle$ (the f-state is considered here). The signal consists of the total fluorescence from this state, detected as a function of pump-probe delay. If not stated differently, we use a 570 nm pump pulse and wave lengths of 310, 330, 340 nm for the probe laser. Assuming a Gaussian envelope function $\exp(-t^2/2\tau^2)$ the temporal width (full-width-at-half-maximum) is $2\tau\sqrt{2\ln 2}$. Since the experimental definition

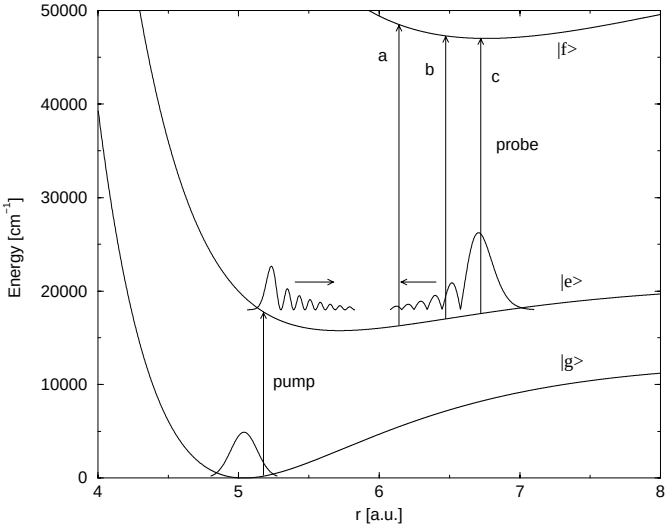

Fig. 1. Pump-probe excitation scheme for the I_2 molecule. Shown are potentials corresponding to the ground ($|g\rangle$ = X), an excited ($|e\rangle$ = B), and an ion-pair electronic state ($|f\rangle = f$), from which fluorescence is detected. The arrows indicate the center wavelengths of the pump (570 nm) and probe (310 nm (a), 330 nm (b), 340 nm (c)) femtosecond pulses. Schematically shown are the initial vibrational state in the $|g\rangle$-state, and the wave packet at the turning points in the $|e\rangle$-state.

of the pulse width is based on the measurement of the intensity autocorrelation function we take $\tau = \tau_{\rm exp}/(2\sqrt{\ln 2})$ in our definition of the pulse width. The potential energy curves for the electronically excited states were taken from references [39,40]. For the ground state (X-state) we used the harmonic approximation to the Morse potential given in reference [41] (ω = 213.6 cm^{-1}, r_0 = 5.038 a.u.). A spatial grind of 2 048 points in the interval [4 a.u., 9 a.u.] was employed in the quantum propagation which was performed with the Split-Operator method [42]. The classical equations of motion are integrated with the velocity Verlet algorithm [19]. The time-step was chosen to be 2 fs in the quantum as well as the classical calculation. The pump-probe signals calculated by classical mechanics were averaged over 20 000 trajectories.

4.2 The pump-transition

Let us, in this subsection, discuss the relation between the quantum mechanical probability distributions and their classical counterparts obtained in the pump-excitation process. In Figure 2 we compare the density $|\Psi_e(r,0)|^2$ calculated within the SF approximation (dotted line), with the numerically exact one (solid line). Whereas for a 20 fs pulse, a reasonable agreement is found, the figure shows that the SF approximation fails drastically for the longer pulse length of 60 fs. First of all, a prominent nodal structure, as visible in the exact solution, is not reproduced. The latter results from quantum-mechanical interference effects which arise from the coherent sum of the amplitudes for photon absorption at different times during the

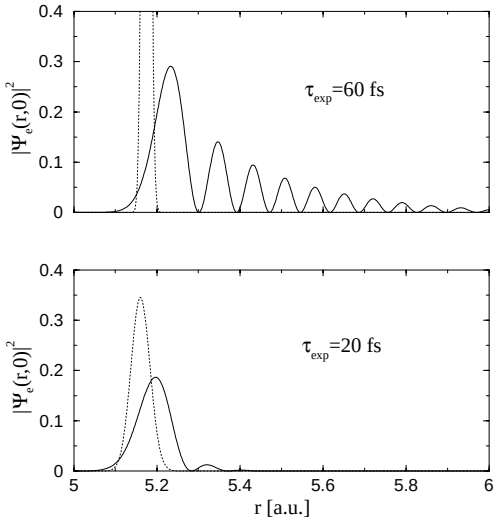

Fig. 2. Vibrational wave packets $|\Psi_e(r,0)|^2$ after pump excitation with a 520 nm pulse of different width, as indicated. The solid line shows wave packets calculated exactly, the dotted line corresponds to wave functions calculated within the SF approximation.

pump–interaction [43]. Besides the lack of the structure in the SF-density, it becomes more localized with increasing pulse width. The opposite is true for the exact density which becomes more delocalized. The latter effect is obviously due to the quantum dynamics in the excited state.

It is clear that the classical distribution function calculated within the SF approximation (Eq. (34)) and regarded as a function of r corresponds exactly to the quantum mechanical density obtained within the same approximation. Thus it suffers from the same deficiencies. The effect of molecular motion during the laser excitation is taken into account by using the time sampling as described in Section 3.3. To give a more instructive insight into the phase-space picture, we plot the Wigner transform of the exact wave function $\Psi_e(r,0)$ and the distribution of classical particles calculated according to equation (43) in Figure 3. We observe that the classical density covers the region of the largest maximum of the Wigner function. An increase of the pulse width leads to the spreading of both the quantum-mechanical and classical function in phase space. The spread of the classical distribution is due to the time sampling giving rise to phase-space points located at different distances, dependent on the time they are generated. Naturally, the quantum mechanical oscillations cannot be seen in the classical function. A second effect is a narrowing of the ridge of the classical distribution with increasing pulse width. This is a result of a smaller window function obtained for longer pulses, limiting the initial positions of trajectories. It is noteworthy that in the limit of continuous wave excitation the present picture is similar to Figure 4a of Heller's paper devoted to classical models of photodissociation dynamics [44].

Figure 4 compares the quantum mechanical spatial density with the classical coordinate distribution function (obtained *via* integration over momentum and sampled

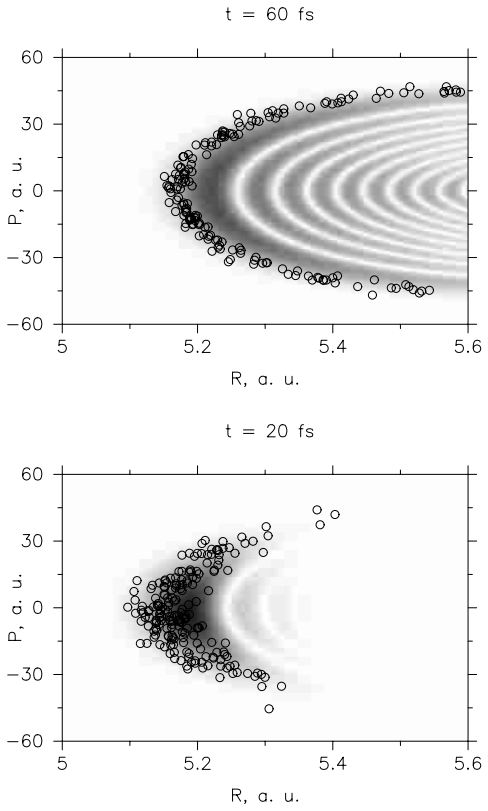

Fig. 3. The Wigner function of the exact wave packet $\Psi_e(r,0)$ as displayed in Figure 2, is compared with a distribution of 200 classical phase-space points sampled from equation (43) and propagated to the time origin. Shown is the modulus of the Wigner function.

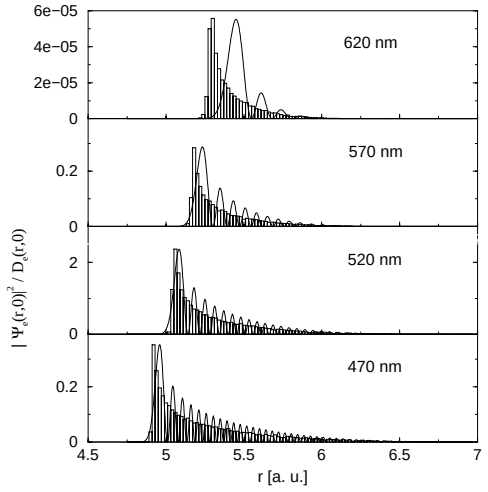

Fig. 4. Coordinate probability functions $|\Psi_e(r,0)|^2$ after excitation with a 60 fs pump pulse are compared with classical coordinate distribution-functions. The pump-pulse wavelength was varied, as indicated. The classical distribution functions are shown as histograms over 20 000 initial configurations.

according to Eq. (43)). The classical function is in good agreement with the quantum-mechanical probability function averaged over the oscillating structure. In fact, pump-probe signals behave similarly in the sense that only an integrated density is measured. This suggests that the classical model could be reliable in the calculation of pump-probe signals, at least for times before purely quantum mechanical features like revivals are encountered (see below). Figure 4 contains curves calculated for different pump-pulse wavelengths. In the case of non-resonant excitation (620 nm wavelength, as commonly used in experiments) the classical and quantum-mechanical distributions are apparently centered at different points. Note that the point obtained for a vertical transition corresponds to the maximum of the classical particles distribution. Moreover, the same effect can be found in Figure 2 that shows a wave packet calculated exactly and within the SF approximation. The outward shift of the quantum-mechanical distribution compared to classical one is well known and can be understood using a linear approximation of the potential curve [26].

4.3 Calculations of pump-probe signals

In order to illustrate differences between approximate and exact calculations of the probe excitation we performed *quantum-mechanical* calculations of the signals. The initial wave function was calculated exactly for a laser wavelength of 570 nm and a pulse duration of 60 fs. The probe wavelength was set to three values (310, 330, and 340 nm) in order to explore different locations of the probe window ranging from the middle to the outer turning point of the wave packet trajectory (see Fig. 1). The probe-pulse width was set to 60 fs as well. Each panel of Figure 5 shows signals calculated exactly (solid line), within the SF- (long dashed line), the MM- (dashed line) and the STF-method (dotted line). As expected from our theoretical analysis the convolution formula gives, in general, the best agreement with the exact pump-probe signal.

In Figure 6 we compare classically and quantum-mechanically calculated signals for the same pulse parameters as used for the results displayed in Figure 5. The quantum-mechanical treatment of the pump- and probe-transitions was performed exactly. The wave function $\Psi_e(r, 0)$ was normalized after the pump excitation was completed. The classical distribution was sampled according to equation (43) and the probe excitation was treated using the STF formula (Eq. (45)). In general, the classical pump-probe spectra (dotted line) are in good agreement with quantum-mechanical ones (solid line). Upon variation of the probe-pulse wavelength, signals calculated by classical and quantum-mechanical approaches behave similarly. However, with the course of time, the classical signal runs more and more ahead corresponding to longer vibrational periods. We explain such a behavior with the help of Figure 4 which shows that the classical initial distribution is shifted towards shorter distances corresponding to a higher potential energy. Due to the potential anharmonicity, the classical distribution thus has a lower average vibrational frequency (96.7 cm^{-1} *vs.* 99.3 cm^{-1} for the quantum-mechanical wave packet). Thus, we show that the effect of the initial state representation on the pump-probe signals exists but it is, in general, small. In passing by, we note that we were not able to obtain a better agreement between the classical and quantum-mechanical results. This is in contradiction to what was found by Li *et al.* [8]. As a main reason, our initial wave packet has an oscillatory structure and differs from the corresponding classical distribution, while the picture presented in reference [8] shows practically an identical initial quantum and

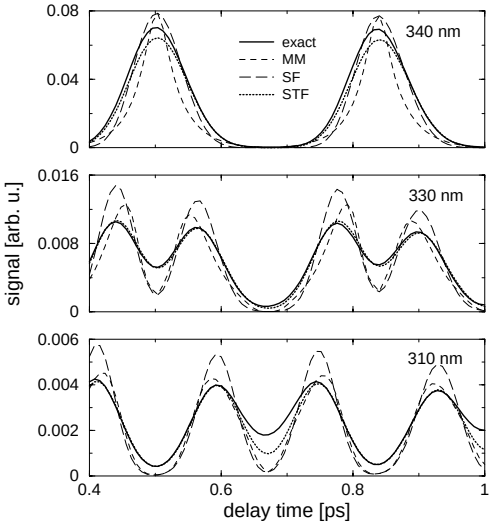

Fig. 5. Pump-probe signals calculated quantum-mechanically for a 570 nm pump pulse and various probe-pulse wavelengths, as indicated (60 fs pulses). The solid line shows the exact quantum-mechanical solution, which is compared to the various approximations, as indicated.

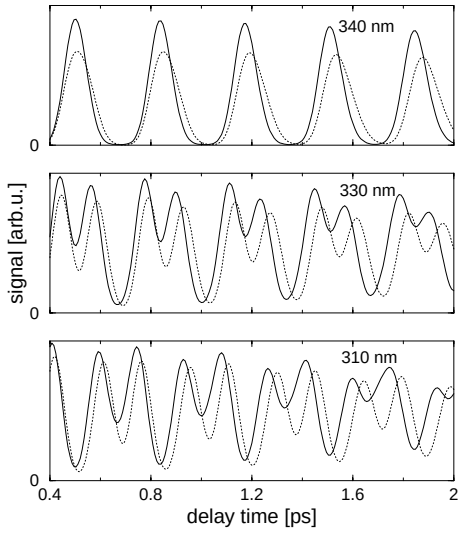

Fig. 6. Pump-probe signals calculated quantum-mechanically (solid line) and classically (dotted line) are compared for an excitation with 60 fs pump- and probe-pulses. The pump excitation wavelength is 570 nm, and various probe wavelengths were used.

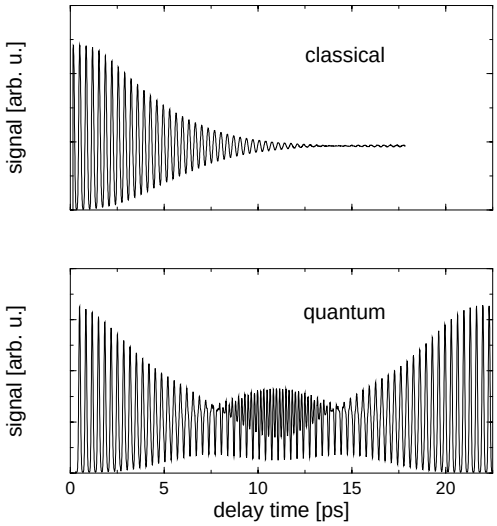

Fig. 7. Classical (upper panel) and quantum (lower panel) pump-probe signals calculated for 570 nm/340 nm laser pulses of 60 fs width are shown on a long time-scale.

classical density in the electronic B-state. Also, Shen and Cina [9] reported large deviations between classical and quantum mechanical densities. The reason is that, opposite to the work presented in reference [8] and the present work, the time-sampling (see Eq. (43)) was not performed.

Finally, in Figure 7 we compare the long-time quantum and classical evolution, as reflected in a pump-probe signal. The re-focusing of the quantum-mechanical wave packet leading to a revival of the signal cannot be reproduced by a purely classical scheme. This is clear since revivals are due to the quantization of energy and are not present in the harmonic case [45]. On the other hand, the classical approach is necessary for a description of systems which consist of many particles. In this case, interactions in the system destroy the quantum coherence, therefore the classical method should generally perform better for more complex cases than for an isolated system.

5 Conclusion

Our results give a general support for using classical mechanics in theoretical considerations of femtosecond experiments. An important point is the accurate representation of the initial state prepared by the pump pulse. Time sampling during the pump excitation is proved to be a sound approach, the agreement improves for a resonant excitation and for shorter pulses.

The Wigner phase-space method employed here for a pure state, applies equally well to incoherent states. For the harmonic oscillator, the statistical sum of the Wigner functions calculated from the oscillator eigenfunctions gives a Boltzmann distribution in the classical limit [31]. Therefore sampling over the classical configuration space using the Boltzmann distribution-function $w(r,p) = \exp(-(p^2/2m + U_g(r))/k_{\mathrm{B}}T)$ can be considered as a classical equivalent to the thermal sum over initial vibrational states in the quantum-mechanical treatment. It is noteworthy that quantum and classical statistics converge in the high temperature limit.

In summary, based on an approximate quantum-mechanical description of optical transitions we have developed a classical scheme for the simulation of femtosecond pump-probe experiments. The classical theory has been tested versus quantum-mechanical calculations using the isolated I_2 molecule as an example. We have, in the meantime, applied the here formulated classical approach to various situations where an anharmonic oscillator interacts with a surrounding. We have first simulated collision-induced recombination of I_2 in Ar [46]. In the corresponding femtosecond experiment [38], the pump pulse excites molecules above the dissociation threshold, and subsequent collisions with Ar lead to the appearance of an oscillatory background in the pump-probe signal. The simulation shows that these features originate from the regular structures in the time-dependent radial I–I distribution function. An analysis of the phase-space picture gives us an interpretation of the structures in terms of caustics [46,47]. We have also investigated the relaxation of a bound-state vibrational wave packet, introducing a novel "phase-energy" approach to the vibrational relaxation problem [48]. In the both cases, the classical simulation has not only helped to elucidate mechanisms of the underlying physical processes, but has also shown how collision processes are reflected in the time-resolved signals (see also Ref. [49]). In any of the former cases we found excellent agreement with experimental results indicating that in many situations a classical approach to simulate transient spectroscopy is worthwhile to undertake.

This work was supported by the Deutsche Forschungsgemeinschaft (Schwerpunktprogramm "Time-dependent phenomena and methods in quantum systems of physics and chemistry") and by the Fonds der Chemischen Industrie.

References

1. A.H. Zewail, *Femtochemistry* (World Scientific, Singapore, 1994), Vols. 1, 2.
2. *Femtosecond Chemistry*, edited by J. Manz, L. Wöste (VCH, Weinheim, 1995).
3. *Chemical Reactions and their Control on the Femtosecond Time Scale*, edited by P. Gaspard, I. Burghardt, Adv. Chem. Phys. **101** (1997).
4. *Femtochemistry*, edited by M. Chergui (World Scientific, Singapore, 1996).
5. *Femtochemistry and Femtobiology*, edited by V. Sundström (World Scientific, Singapore, 1997).
6. A.H. Zewail, J. Phys. Chem. **104**, 5660 (2000).
7. *The Physics and Chemistry of Wave Packets*, edited by J. Yeazell, A.T. Uzer (Wiley, New York, 2000).
8. Z. Li, J.-Y. Fang, C.C. Martens, J. Chem. Phys. **104**, 6919 (1996).
9. Y.-C. Shen, J.A. Cina, J. Chem. Phys. **110**, 9793 (1999).

10. J. Che, W. Zhang, Y.J. Yan, J. Chem. Phys. **106**, 6947 (1997).
11. H. Dietz, V. Engel, J. Phys. Chem. A **102**, 7406 (1998).
12. R. Zadoyan, Z. Li, P. Ashjian, C.C. Martens, V.A. Apkarian, Chem. Phys. Lett. **218**, 504 (1994).
13. C.J. Bardeen, J. Che, K.R. Wilson, V.V. Yakovlev, V.A. Apkarian, C.C. Martens, R. Zadoyan, B. Kohler, M. Messina, J. Chem. Phys. **106**, 8486 (1997).
14. R. Zadoyan, M. Sterling, M. Ovchinnikov, V.A. Apkarian, J. Chem. Phys. **107**, 8446 (1997).
15. R.E. Walkup, J.A. Misewich, J.H. Glownia, P.P. Sorokin, Phys. Rev. Lett. **65**, 2366 (1990).
16. R.E. Walkup, J.A. Misewich, J.H. Glownia, P.P. Sorokin, J. Chem. Phys. **94**, 3389 (1991).
17. L.E. Fried, S. Mukamel, J. Chem. Phys. **93**, 3063 (1990).
18. V.A. Ermoshin, A.K. Kazansky, V. Engel, J. Chem. Phys. **111**, 7807 (1999).
19. M.P. Allen, D.J. Tildesley, *Computer Simulations of Liquids* (Oxford University Press, Oxford, 1989).
20. R. Bersohn, A.H. Zewail, Ber. Bunsenges. Phys. Chem. **92**, 373 (1988).
21. M. Lax, J. Chem. Phys. **20**, 1752 (1952).
22. E. Wigner, Phys. Rev. **40**, 749 (1932).
23. E. Wigner, M. Hillery, R.F. O'Connell, M.O. Scully, E.P. Wigner, Phys. Rep. **106**, 121 (1984).
24. W.P. Schleich, *Quantum Optics in Phase Space* (Wiley-VCH, Berlin, 2001).
25. W.H. Louisell, *Quantum Statistical Properties of Radiation* (John Wiley & Sons, 1990).
26. R. Schinke, *Photodissociation dynamics* (Cambridge University Press, Cambridge, 1993).
27. E.M. Hiller, J.A. Cina, J. Chem. Phys. **105**, 3419 (1996).
28. J. Cao, J. Che, K.R. Wilson, J. Phys. Chem. A **102**, 4284 (1998).
29. S. Meyer, C. Meier, V. Engel, J. Chem. Phys. **108**, 7631 (1998).
30. R.G. Parr, W. Yang, *Density-Functional Theory of Atoms and Molecules* (Oxford University Press, Oxford, 1989).
31. J.P. Dahl, in *Conceptual Trends in Quantum Chemistry*, edited by E.S. Kryachko, J.L. Calais (Kluwer Academic Publishers, 1994), pp. 199-226.
32. E.J. Heller, J. Chem. Phys. **65**, 1289 (1976).
33. N.E. Henriksen, G.D. Billing, F.Y. Hansen, Chem. Phys. Lett. **149**, 397 (1988).
34. K. Singer, W. Smith, Chem. Phys. Lett. **167**, 298 (1990).
35. K.B. Møller, J.P. Dahl, N.E. Henriksen, J. Phys. Chem. **98**, 3272 (1994).
36. R.M. Bowman, M. Dantus, A.H. Zewail, Chem. Phys. Lett. **161**, 297 (1989).
37. M. Gruebele, A.H. Zewail, J. Chem. Phys. **98**, 883 (1993).
38. C. Wan, M. Gupta, J.S. Baskin, Z.H. Kim, A.H. Zewail, J. Chem. Phys. **106**, 4353 (1997).
39. M. Ben-Nun, R.D. Levine, D.M. Jonas, G.R. Fleming, Chem. Phys. Lett. **245**, 629 (1995).
40. P. Perrot, A.J. Bouvier, A. Bouvier, B. Femelat, J. Chevaleyre, J. Mol. Spectrosc. **114**, 60 (1985).
41. J.-Y. Fang, C.C. Martens, J. Chem. Phys. **105**, 9072 (1996).
42. M.D. Feit, J.A. Fleck, A. Steiger, J. Comp. Phys. **47**, 412 (1982).
43. C. Meier, V. Engel, in reference [2], Chapter 11.
44. E.J. Heller, J. Chem. Phys. **68**, 2066 (1978).
45. I. Sh. Averbukh, N.F. Perelman, Phys. Lett. A **139**, 449 (1989).
46. V.A. Ermoshin, V. Engel, C. Meier, J. Chem. Phys. **113**, 6585 (2000).
47. V.A. Ermoshin, V. Engel, C. Meier, J. Chem. Phys. **113**, 5770 (2000).
48. A.K. Kazansky, V.A. Ermoshin, V. Engel, J. Chem. Phys. **113**, 8865 (2000).
49. V.A. Ermoshin, V. Engel, Z. Phys. Chem. **214**, 1265 (2000).